

Rippled quasi-perpendicular collisionless shocks: Local and global normals

L. Ofman^{1,2} and M. Gedalin³

Received 19 February 2013; revised 1 October 2013; accepted 6 October 2013; published 23 October 2013.

[1] Proper determination of the shock normal is necessary for reliable determination of observed heliospheric shock parameters and comparison of observations with theory. The existing methods work sufficiently well for low and moderate Mach numbers one-dimensional stationary shocks. Higher-Mach-number shocks are no longer planar at the scales of the ion convective gyroradius or smaller. In rippled shock fronts, the local shock normal may differ substantially from the global normal. The former is determined by the local direction of the fastest variation of the magnetic field, while the latter is determined by the far upstream and far downstream plasma conditions. Here we use 2-D hybrid modeling of quasi-perpendicular collisionless shocks with moderate and high Mach numbers to quantify the difference between the directions of the two normals. We find that the angle between the local normal and the global normal may be as large as 40° within the front of a rippled heliospheric shock. The coplanarity method of the shock normal determination is sensitive to the choice of the region for the magnetic field averaging. We also find that the usage of the sliding averaging region in the close vicinity of the shock transition provides satisfactory estimates of the global normal.

Citation: Ofman, L., and M. Gedalin (2013), Rippled quasi-perpendicular collisionless shocks: Local and global normals, *J. Geophys. Res. Space Physics*, 118, 5999–6006, doi:10.1002/2013JA018780.

1. Introduction

[2] The angle between the shock normal and the upstream magnetic field is one of the basic shock parameters. Many of the shock properties depend crucially on this angle, and the knowledge of this parameter is vital for comparison of theory with spacecraft observations. The speed of the magnetosonic wave and, respectively, the corresponding Mach number depends on this angle. The foot length and the noncoplanar magnetic field magnitude, as well as the ion reflection process and the ion ability of escape upstream depend on the shock obliquity. Errors in the determination of the shock normal would affect proper evaluation of the normal component of the shock velocity relative to the upstream plasma, bringing about errors in the determination of the Mach number, of the conversion of temporal measurements into spatial ones, of the path along which the shock is crossed, to list only the most obvious affected parameters. Hence, the necessity of reliable determination of the shock normal from the in situ measurements available in the heliosphere. Indirect determination of the shock normal is possible for steady (on the timescale of at least several ion gyroperiods) shocks, like planetary bow shocks [Horbury

et al., 2002] and involves usage of the global model for the shock surface. This method cannot be applied to transient shocks, like interplanetary ones. Direct determination is typically based on application of the coplanarity theorem and/or Rankine-Hugoniot relations to single spacecraft or multispacecraft measurements of the magnetic field and particle distributions [Abraham-Shrauner, 1972; Russell *et al.*, 1982; Scudder *et al.*, 1986; Viñas and Scudder, 1986; Mazelle *et al.*, 2010]. The latter are often of limited use because of lower temporal resolution and poor resolution of the cold solar wind beam. More sophisticated methods are available for simultaneous multispacecraft measurements [Dunlop *et al.*, 2002; Horbury *et al.*, 2001, 2002]. These methods imply shock planarity at the scale of the spacecraft separation.

[3] Both coplanarity theorem and Rankine-Hugoniot relations refer to the asymptotically homogeneous and to upstream and downstream gyrotropic states. While it is easy to have these asymptotic regions in theory and numerical simulations, in observed shocks, both upstream and downstream regions may not reach a uniform state. The upstream region may be “contaminated” with waves propagating toward the shock [see, e.g., Greenstadt *et al.*, 1975; Russell *et al.*, 1982]. Ion distributions gyrotropize slowly behind the shock [Schkopke *et al.*, 1983], and large amplitude magnetic oscillations may persist well into downstream [Balikhin *et al.*, 2008; Russell *et al.*, 2009]. Upstream and downstream regions, available for the analysis, may be limited by, for example, a rotational discontinuity close to the shock front [Scudder *et al.*, 1986] or the magnetic pileup boundary positioned too close to the (Venusian) shock transition [Walker *et al.*, 2011]. Thus, in many cases, one has to

¹CUA and NASA/GSFC, Code 671, Greenbelt, Maryland, USA.

²Visiting Associate Professor, Tel Aviv University, Tel Aviv, Israel.

³Department of Physics, Ben-Gurion University of the Negev, Beer-Sheva, Israel.

Corresponding author: L. Ofman, CUA and NASA/GSFC, Code 671, Greenbelt, MD 20771, USA. (Leon.Ofman@nasa.gov)

determine the shock normal based on the measurements of rather short upstream and downstream regions adjacent to the shock ramp. Moreover, the local direction of the largest gradient of the magnetic field is also of interest since the local field geometry affects the particle motion in the ramp and thus determines the features of reflected and transmitted ion distribution as well as the electron distributions. Thus, the local normal determination is also important. This task is also complicated by, for example, a noticeable noncoplanar component of the magnetic field that appears inside the shock transition [Gedalin, 1996] due to the nongyrotropy of the ion distribution upon the shock crossing [Skopke et al., 1983; Burgess et al., 1989; Skopke et al., 1990] and the nondiagonal nature of the ion pressure tensor [Li et al., 1995; Gedalin and Zilbersher, 1995; Gedalin and Balikhin, 2008]. Yet because of the high quality of the magnetic field measurements, the most frequent approach remains using the coplanarity of the upstream and downstream mean magnetic fields and constancy of the normal component [Newbury et al., 1998]. Since the magnetic field profile is rarely monotonic and often contains large upstream oscillations just ahead of the ramp and/or large downstream oscillations just behind the ramp [Balikhin et al., 2008; Russell et al., 2009], the method requires careful choice of the upstream and downstream regions for averaging. In many cases, the choice is difficult since oscillations persist well across the shock to the region where the structure cannot be assumed one-dimensional any longer. In particular, this problem arises when determining the normal to the bow shocks at nonmagnetized planets (Venus and Mars), where the whole magnetosheath may be of the order of several gyroradii [Walker et al., 2011]. Rippling can develop on the flanks of Coronal Mass Ejections (CME's) driven shocks due to inhomogeneity in the background solar wind [e.g., Bale et al., 1999] that can modulate the excited radio emission and affect the dynamic spectra of type-II radio bursts as has been shown with the aid of MHD modeling [e.g., Schmidt and Cairns, 2012]. However, MHD modeling is limited to large-scale rippling (i.e., \gg ion inertial length), and cannot properly describe the growth of rippling due to kinetic instabilities and the associated ion gyromotions. Two-dimensional hybrid modeling is necessary in order to study the small-scale quasi-perpendicular shock front rippling properties [e.g., Winske and Quest, 1988; Burgess, 2006].

[4] A number of different rippling regimes have been discussed, mostly within numerical simulations. Using 2-D hybrid simulations, Winske and Quest [1988] found in 2-D spatially periodic modulations of the planar shock surface with the maximum-to-maximum length of about six ion inertial lengths. The rippling was shown to occur in the high-Mach-number regime, $M_A > 6$, and it was suggested that ion pressure anisotropy caused modes/instabilities are responsible for the rippling. Later, rippling on similar scales was found by Lowe and Burgess [2003]; Burgess and Scholer [2007] using 2-D hybrid simulations and attributed to the surface waves developing due to the instability associated with reflected ions. Observations by [Moullard et al., 2006; Lobzin et al., 2008] confirmed the existence of this type of rippling. Large-scale rippling with the wavelength of about 20 ion inertial lengths was found in numerical simulations by Yuan et al. [2009]. In that study the wavelength

was comparable to the simulation region width (30 ion inertia lengths).

[5] Small-scale modulations (maximum-to-maximum length of a fraction of the ion inertial length) have been observed in particle-in-cell (PIC) simulations [Lembège and Savoini, 1992; Savoini and Lembege, 1994; Lembège et al., 2009; Yang et al., 2012]. In these studies the box width was only several ion inertial lengths, and large-scale modulations could not be reliably modeled. Present computational limitations of PIC codes force to use the set of parameters for which the Alfvén-to-light speed ratio is by about two orders of magnitude higher than in the heliosphere. The similarity of the modeled shocks to the observed ones in these very different parameter regimes is yet to be shown [Krasnoselskikh et al., 2013].

[6] Rippling with a much larger scale ($\sim 100c/\omega_{pi}$) than in the present study due to upstream waves is described by Krauss-Varban et al. [2008]. Finally, variations of the solar wind parameters, like heliolongitude variations of the IMF direction, would affect the shock surface. The scale of these variations are expected to be even larger. In the present paper we study the rippling which is produced by the ion dynamics at the shock front and adopt the point of view of Lowe and Burgess [2003]; Burgess et al. [1989] (see also the review by Hellinger [2003]) that modulation of the shock surface is a result of surface instability.

[7] Nonstationarity of the shock, especially reformation [Matsukiyo and Scholer, 2006; Lobzin et al., 2007; Lefebvre et al., 2009; Mazelle et al., 2010], complicates the task even further. In the case of stationary shocks with ripples [Lowe and Burgess, 2003; Burgess, 2006; Moullard et al., 2006; Burgess and Scholer, 2007], one may distinguish between the global normal, which is ideally determined by the far upstream and far downstream states and the local normal. The latter differs from the global one since the shock front is no longer planar. In magnetohydrodynamics, a shock front would be described by a surface where a discontinuous magnetic field jump occurs. Natural generalization of this description to real finite width shocks would be defining the surface of the constant magnetic field magnitude, $|\mathbf{B}| = \text{const}$. Accordingly, the local normal direction is given by $\hat{\mathbf{n}}_l = \nabla B / |\nabla B|$. While this local normal can be determined everywhere through the shock, it is of direct physical sense in the regions with the largest magnetic field gradients and magnetic field changes, like the ramp and larger amplitude downstream oscillations (if any), with small-scale fluctuation effects excluded. It is the global normal which is eventually related to Rankine-Hugoniot relations, but it is the local normal which is related to the shock fine structure and the field governing the important particle dynamics, like ion reflection and electron heating. Knowledge of the global normal is necessary for proper identification of the upstream parameters, while knowledge of the local normal is essential for proper understanding of the particle dynamics inside the shock transition layer. The latter is important for understanding the ion and electron heating and acceleration processes. Of particular interest is the local normal in the ramp, since there the gradients are the largest.

[8] Recently, Ofman and Gedalin [2013] studied quasi-perpendicular collisionless shock dynamics using 2-D hybrid simulations and investigated the gyrating downstream ion distributions for low- and high-Mach-number

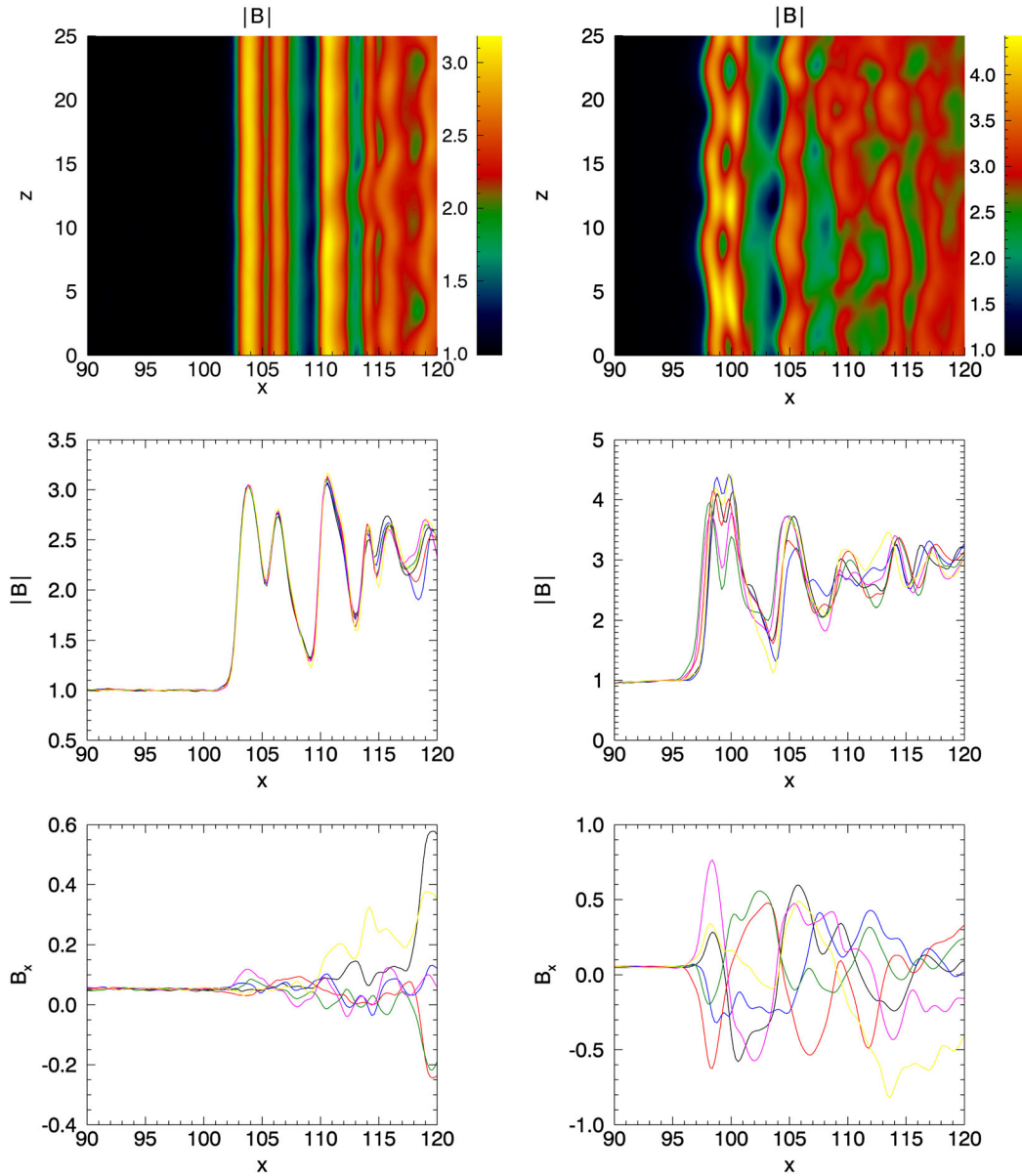


Figure 1. The magnetic field magnitude $|B|$ for the case (left column) $M = 3.4$ and (right column) $M = 4.7$, $\beta_e = \beta_i = 0.4$. (top row) Filled contour plot of the magnetic field magnitude. (middle row) A number of cuts of $|B|$ for $z = 2.6$ (black), $z = 4.42$ (blue), $z = 6.24$ (red), $z = 8.06$ (green), $z = 9.88$ (magenta), and $z = 11.7$ (yellow). (bottom row) Cuts of B_x for the same z .

shocks. In this paper we focus our 2-D hybrid study on the deviations of the local normal from the global one due to rippling of high-Mach-number shocks. We show quantitatively for the first time that the two may differ substantially and estimate the errors due to the standard methods of the normal determination applied to rippled shocks.

2. Simulation Setup

[9] In order to study the shock profile, we performed 2.5-D hybrid simulations (in two spatial dimensions with all three components of the velocities and fields). The approach is rather standard and basically follows that of *Winske and Quest* [1988], extended here by nearly two orders of magnitude larger number of particles and higher resolution, thanks

to the advances in the present day computing resources and parallel programming. Below, we describe for completeness briefly the modeling method—further details can be found in *Ofman and Gedalin* [2013, and references therein]. Almost perpendicular geometry, $\cos \theta = 0.05, 0.17$ was chosen, where θ is the angle between the shock normal and the upstream magnetic field. In such geometry the noncoplanar component of the magnetic field is expected to be small. The errors in the determination of the shock normal direction are not small in this case because of the substantial effect of the fluctuations at the background of the weak normal component of the magnetic field. Thus, the effects due to rippling should be significantly larger to be distinguished from the fluctuation induced uncertainty. The upstream magnetic field was taken to lie in the plane of the simulation. In what

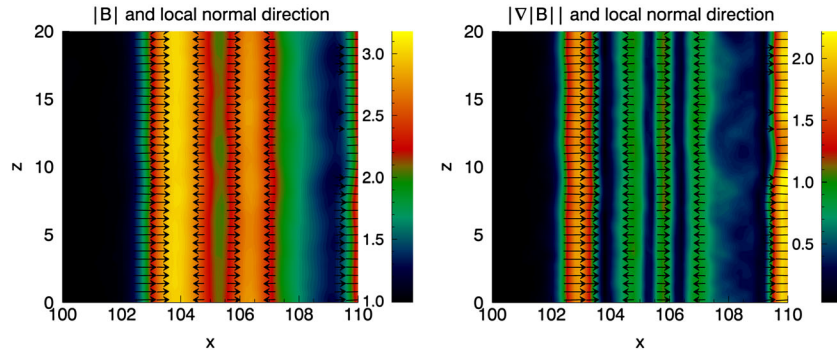


Figure 2. (left) The magnetic field magnitude and the local normal direction for the planar shock ($M = 3.4$, $\beta_e = \beta_i = 0.4$). (right) The magnitude of the gradient of the magnetic field magnitude (arbitrary relative units) and the local normal direction for the same shock. The normal direction is shown for the regions where $|\nabla|B|| > 0.65$ while $|\nabla|B||_{\max} = 2.2$.

follows, we denote the coordinate along the shock normal by x , the simulation plane is $x - z$, and y is along the noncoplanarity direction. Electrons were treated here as a massless isothermal fluid, while protons were treated as particles. The electron and proton upstream temperatures are equal, so that $\beta_e = \beta_i$ (where “ i ” indicates protons “ p ” in this study). The spatial resolution was typically 1024×128 cells with grid size of 0.2×0.2 in units of ion inertial length c/ω_{pp} , where $\omega_{pp} = (4\pi n_p e^2/m_p)^{1/2}$ is the proton plasma frequency. We used 200 particles per cell on average in the 2-D computational domain with a total of ~ 26 million particles. The 2-D hybrid code is parallelized, allowing rapid execution on multiple processors (typically 256 to 512). Each model particle is in fact a “super-particle” representing many physical particles with the same position in phase space with the ratio between them determined by density normalization. The equations of motion for the particles were integrated at each time step. The velocities and the positions were used to calculate the currents and the charge density, which were in turn used to calculate the fields from Maxwell’s equations. The boundary conditions across the flow, in the z direction, were periodic. In the flow direction, x , the upstream plasma was injected at one boundary and reflected at the other, so that the shock formed by the collisionless interaction between the impacting plasma and the reflected stream (similar approach was utilized by *Ofman et al.* [2009] in 1-D and *Ofman and*

Gedalin [2013] in 2-D hybrid studies). Simulations were run up to the point where the shock structure was fully developed (typically ~ 20 proton gyroperiods). The field solutions were obtained using finite differences for spatial derivatives and the Rational Runge-Kutta (RRK) method [*Wambeq, 1978*] for temporal integration.

3. Results

[10] A number of runs have been performed with moderate and high Mach numbers and upstream β . For comparison, we present here a one-dimensional shock and a rippled shock with $\beta_e = \beta_i = 0.4$. Figure 1 shows the magnitude of the magnetic field for a nearly perpendicular shock with the Alfvénic Mach number $M = 3.4$ (Figure 1, left column, no rippling) and $M = 4.7$ (Figure 1, right column, rippling present), $\beta_e = \beta_i = 0.4$, and $\cos \theta = 0.05$ (contour plot of Figure 1, top row). In what follows, all coordinates are normalized to the ion inertial length c/ω_{pi} , where $\omega_{pi}^2 = 4\pi n_u e^2/m_i$, and n_u is the upstream ion number density. The magnetic field is normalized on the upstream magnetic field B_u . The shock transition occurs at $x \approx 103$. The cuts of $|B|$ at various z (Figure 1, middle row) show that the shock is one-dimensional with only weak fluctuations in the vicinity of the transition. This can be also seen from the cuts for B_x (Figure 1, bottom row): substantial fluctuations start at about $x = 110$, more than one upstream

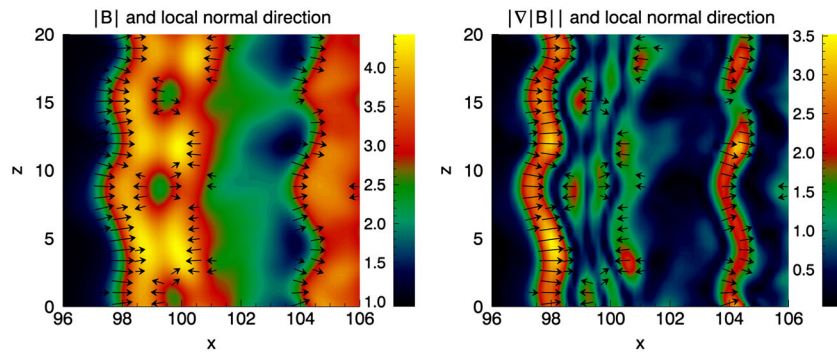


Figure 3. (left) The magnetic field magnitude and the local normal direction for the rippled shock ($M = 4.7$, $\beta_e = \beta_i = 0.4$). (right) The magnitude of the gradient of the magnetic field magnitude (arbitrary units) and the local normal direction for the same shock. The latter is subsampled and shown only in the regions where $|\nabla|B|| > 1.2$, while $|\nabla|B||_{\max} = 3.5$.

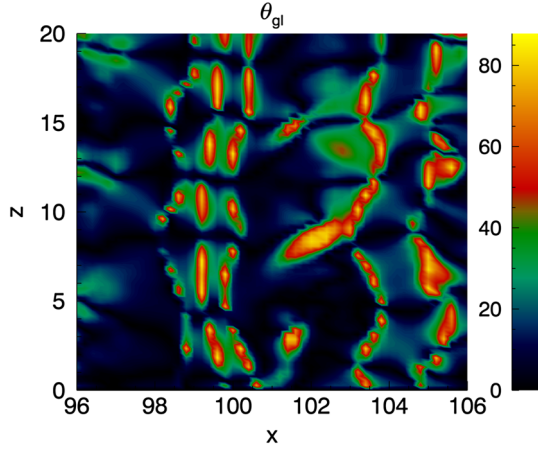


Figure 4. The angle θ_{gl} between the local and the global shock normals for the above rippled shock.

convective gyroradius behind the ramp. Beyond that point the downstream region is affected by the wall. This situation is rather typical for interplanetary shocks and bow shocks at nonmagnetized planets: these shocks may be affected by the presence of other boundaries (like the magnetic pileup boundary) or MHD discontinuities. Large amplitude downstream oscillations of the magnetic field just behind the ramp are related to the nongyrotropy of the ion distribution behind the shock [Balikhin *et al.*, 2008; Ofman *et al.*, 2009; Ofman and Gedalin, 2013] and are components of the shock structure.

[11] Figure 2 shows the magnetic field and the magnetic field gradient for the planar shock, together with the direction of the local normal superimposed. In Figure 2, bottom, the direction of the local normal is evaluated only for the regions where $|\nabla|B|| > 0.65$ (in arbitrary units, where the maximum gradient is ≈ 2.2). Of particular interest is the local normal in the regions of substantial magnetic field changes, for example, the ramp. The physical importance of the local normal is that it is expected to determine the direction of the cross-shock electric field. Indeed, in planar shocks, the electric field along the shock normal in the ramp is given approximately by the following relation [see, e.g., Gedalin, 1996; Gedalin and Balikhin, 2004]

$$E_x = -\frac{B}{4\pi ne} \frac{dB}{dx} - \frac{1}{ne} \frac{dp_e}{dx}, \quad (1)$$

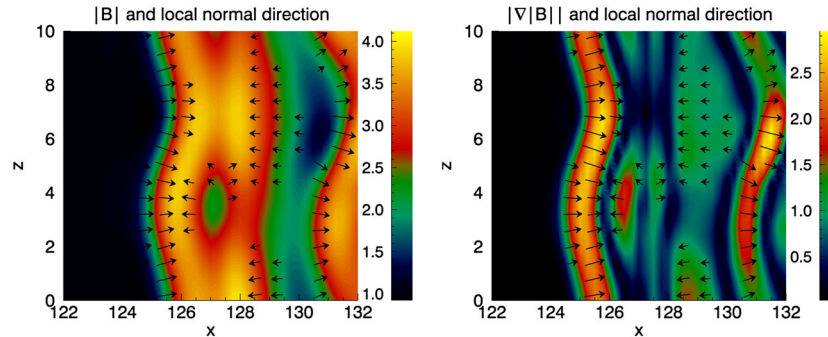


Figure 5. (left) Magnetic field magnitude and direction of the local shock normal in the shock transition vicinity, for the shock with $M = 4.2$, $\beta = 0.4$, and $\theta = 80^\circ$. (right) Magnetic field gradient and the local shock normal for the same shock for $|\nabla|B|| > 0.9$ with $\max |\nabla|B|| \approx 2.95$.

where x is along the shock normal. In the case of a rippled shock d/dx should be replaced with ∇ , within the same approximation, that is, in the ramp vicinity. As expected, in the planar shock, no noticeable deviations of the local normal from the global one are present.

[12] Figure 3 shows a fragment of the rippled shock ($M = 4.7$, $\beta_e = \beta_i = 0.4$), together with the gradient of the magnetic field and the direction of the local normal. Rippling of the shock surface is clearly seen in the spatially varying (along the shock front) position of the ramp and in the nonuniform magnetic field maximum, as well as in the fluctuations of B_x in the shock transition. The wavelength of the rippling (from one leftmost position of the ramp to the nearest one along z axis) is ≈ 5 ion inertial lengths which is of the order of the upstream ion convective gyroradius. The amplitude (the distance from the leftmost position of the ramp to the nearest rightmost position) is about 0.5 of the ion inertial length. The deviations of the local normal from the global one is quantified by presenting the angle θ_{gl} between the two in Figure 4. The local shock normal is calculated as $\nabla|B|/|\nabla|B||$. The small-scale low-amplitude noise was suppressed throughout by replacing $|\nabla|B|| \rightarrow (|\nabla|B||^2 + 0.025)^{1/2}$. The local normal is always in the $x-z$ plane since there is no y dependence in the simulation. The global normal is along x . At the ramp, $x \approx 98$, the angle between the two normals reaches the values 40° .

[13] The above considered shocks are nearly perpendicular. Below we present the analysis of a more oblique rippled shock with $\theta = 80^\circ$ and $\beta = 0.4$. Rippling was achieved at a lower Mach number, $M = 4.2$ (compare with $M = 4.7$ for the nearly perpendicular shock). The relevant part of the shock magnetic field, together with the gradient and the local normal direction, is shown in Figure 5. The wavelength of the rippling along the shock front is about $7(c/\omega_{pi})$, while the amplitude is about one c/ω_{pi} , both slightly larger than in the previously analyzed nearly perpendicular shock. Figure 6 quantifies the deviations of the local shock normal from the global normal. The same reduction of the small-scale noise as above was applied. There are substantial deviations, up to 40° , closely following the surface of the magnetic profile. Figure 7 shows the angle between the local shock normal and the local magnetic field vector. It is worth noting that the deviations are in both directions: parts of the shock surface have locally perpendicular geometry, $\theta_{nB} \approx 90^\circ$, while other parts are more oblique, $\theta_{nB} \approx 50^\circ$,

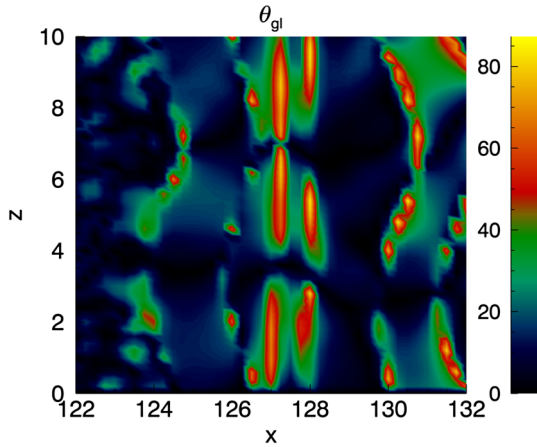


Figure 6. The angle θ_{gl} between the global and the local shock normals for the rippled shock shown in Figure 5.

than would be in a planar shock. Such coexistence of substantially oblique and nearly perpendicular pieces of the shock front may have significant implications for ion and electron motion [Gedalin, 2001; Yang *et al.*, 2012].

[14] The coplanarity method is the most used when the shock normal is to be determined from single spacecraft measurements. The method uses two vectors of the magnetic field obtained by averaging over appropriate upstream and downstream regions. For rippled shocks, one may expect that the result would be sensitive to the choice of the downstream averaging region. In order to quantify this sensitivity, we apply the coplanarity method to a number of downstream intervals. Namely, for each coordinate z (across the simulation box), we use a number of pairs of magnetic vectors. One of the pairs is always the upstream magnetic field vector (easily determined by averaging over a suitable upstream region) and the other one is the magnetic field obtained by averaging over the region $[x, x + 3(c/\omega_{pi})]$, where x is the coordinate along the simulation box. Applying the coplanarity procedure to the pairs for various x , we obtain the coplanarity derived normal as a function of x . Since

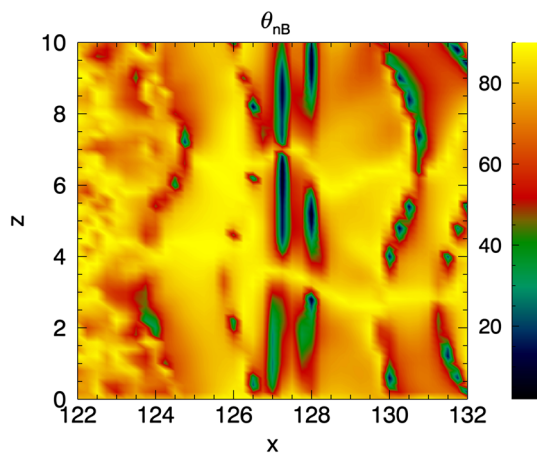


Figure 7. The angle between the local normal and the local magnetic field for the rippled shock with $\theta = 80^\circ$ (the rippled shock shown in Figure 5).

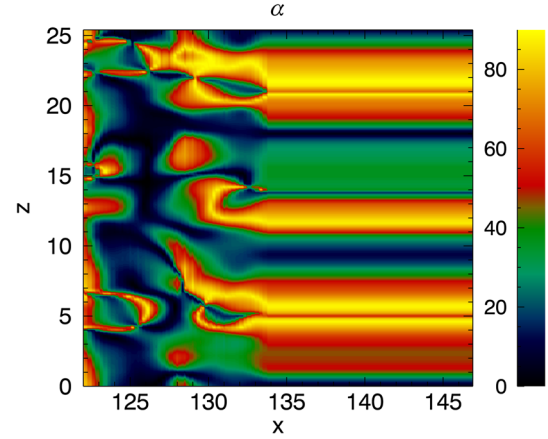


Figure 8. The angle between the sliding coplanarity normal and the global normal for the rippled shock shown in Figure 5.

the downstream averaging region slides along the shock normal, we shall refer to the approach as the sliding coplanarity method and the normal obtained in this way as the sliding coplanarity normal. Figure 8 shows the angle between the sliding coplanarity normal obtained by averaging over $[x, x + 3(c/\omega_{pi})]$ along $z = \text{const}$, and the global normal. The sliding coplanarity normal is reasonably close to the global normal only in the region sufficiently close to the shock transition (within several ion inertial lengths). Choosing the averaging interval further downstream may result in large errors in the determination of the shock normal.

4. Conclusions

[15] The global shock normal refers to the uniform upstream and downstream states and to the Rankine-Hugoniot relations connecting these states. Knowledge of a global shock normal is essential for proper assessment of the basic shock parameters such as the angle between the shock normal and upstream magnetic field. The latter is necessary for the determination of the shock Mach number, which is considered the most important shock parameter. Determination of the global shock normal in a one-dimensional stationary quasi-perpendicular shock from a single spacecraft magnetic field measurements may be complicated by the presence of the downstream oscillations due to the nongyrotropy of the ion distribution upon crossing the shock. Additional difficulties may arise because of a short downstream region available for measurements. Strictly speaking, the coplanarity theorem is not applicable in these cases. Yet rather good estimates can be done by applying the coplanarity method to the field which is averaged over a properly chosen downstream interval, where excursions of the magnetic field from the coplanarity plane may be expected to cancel each other.

[16] In order to overcome this difficulty, one can employ detailed numerical simulations of the shock front topology on the rippling (small) scale. Here we used 2-D hybrid simulations to study moderate- and high-Mach-number quasi-perpendicular collisionless shocks. The former case leads to one-dimensional shock front structure, and the later forms a

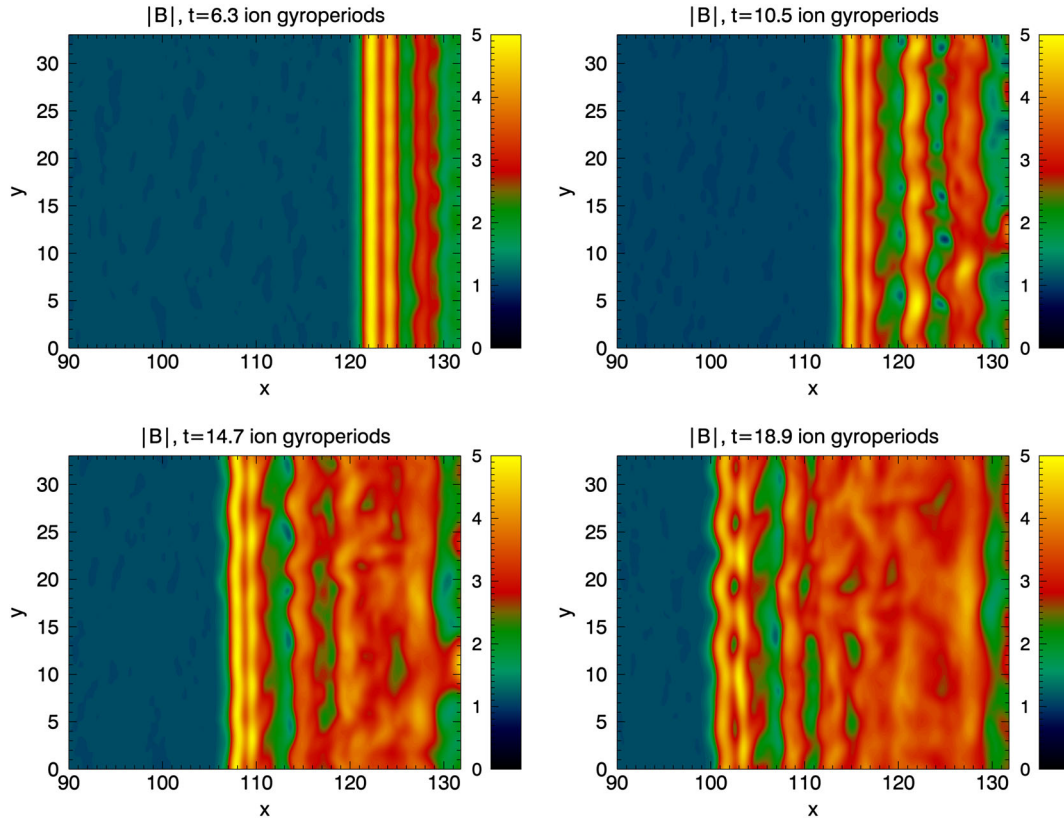


Figure 9. Four snapshots of the magnetic field magnitude, showing the development of the rippling for the shock in Figure 1, right column.

rippled shock front. In planar shocks the local normal coincides with the global normal. In a rippled shock the local normal, defined as the direction of the fastest magnetic field increase, may differ substantially from the global normal. Knowledge of the local normal is essential for understanding the dynamics of the particles, in particular, electrons, inside the shock front. We found that even in the case of weak rippling considered here the angle between the two normals may be as large as 40° . We conclude that there is no apparent way to determine the local normal from single spacecraft measurements. Two-dimensional inhomogeneity persist well beyond the transition layer, which makes the determination of the global shock normal from coplanarity even more difficult. Here we suggest the sliding coplanarity method where the downstream averaging interval slides along the path of the spacecraft, for the determination of the global shock normal. If the obtained shock normal remains approximately constant within several ion inertial lengths just beyond the shock transition, there are good chances that this normal is reasonably aligned to the global normal.

[17] The numerically obtained characteristics of the rippling (wavelength between the ion inertial length and ion convective gyroradius, amplitude about one ion inertial length, and decay toward downstream) show that it is likely to be the result of a corrugation instability of the shock front. Some indications of such instability may be seen from Figure 9, showing the development of the rippling for the shock in Figure 1, right column. Rippling first appears about six ion gyroperiods from the beginning of the run, when

the shock front has already moved sufficiently far from the wall to allow free gyration of the transmitted ions behind the ramp. The appearance of the perturbations slightly downstream of the main magnetic jump is consistent both with the MHD corrugation instability option (no perturbation can occur upstream) and with the plausible scenario where the gyrating distribution of the transmitted ions becomes unstable with respect to modulation along the shock front. At later times the rippling evolves to the stage where the upstream edge of the ramp is not planar anymore. This pattern remains rather stable, while further downstream the rippling decays. In order to shed light on the nature of the instability, these numerical simulations should be complemented with analytical work, which is in progress.

[18] **Acknowledgments.** L.O. would like to acknowledge discussions with A. F. Viñas, and support by NASA grant NNX10AC56G.

[19] Philippa Browning thanks the reviewers for their assistance in evaluating this paper.

References

- Abraham-Shrauner, B. (1972), Determination of magnetohydrodynamic shock normals, *J. Geophys. Res.*, *77*, 736–739.
- Bale, S. D., M. J. Reiner, J.-L. Bougeret, M. L. Kaiser, S. Krucker, D. E. Larson, and R. P. Lin (1999), The source region of an interplanetary type II radio burst, *Geophys. Res. Lett.*, *26*, 1573–1576.
- Balikhin, M. A., T. L. Zhang, M. Gedalin, N. Y. Ganushkina, and S. A. Pope (2008), Venus Express observes a new type of shock with pure kinematic relaxation, *Geophys. Res. Lett.*, *35*, L01103, doi:10.1029/2007GL032495.
- Burgess, D., W. P. Wilkinson, and S. J. Schwartz (1989), Ion distributions and thermalization at perpendicular and quasi-perpendicular supercritical collisionless shocks, *J. Geophys. Res.*, *94*, 8783–8792.

- Burgess, D. (2006), Interpreting multipoint observations of substructure at the quasi-perpendicular bow shock: Simulations, *J. Geophys. Res.*, *111*, A10210, doi:10.1029/2006JA011691.
- Burgess, D., and M. Scholer (2007), Shock front instability associated with reflected ions at the perpendicular shock, *Phys. Plasmas*, *14*, 012108-1–012108-9.
- Dunlop, M. W., A. Balogh, and K.-H. Glassmeier (2002), Four-point Cluster application of magnetic field analysis tools: The discontinuity analyzer, *J. Geophys. Res.*, *107*(A11), 1385, doi:10.1029/2001JA005089.
- Gedalin, M., and D. Zilbersher (1995), Non-diagonal ion pressure in nearly-perpendicular collisionless shocks, *Geophys. Res. Lett.*, *22*, 3279–3282.
- Gedalin, M. (1996), Noncoplanar magnetic field in the collisionless shock front, *J. Geophys. Res.*, *101*, 11,153–11,156.
- Gedalin, M. (2001), Influence of the rippling on the collisionless ion and electron motion in the shock front: A model study, *J. Geophys. Res.*, *106*, 21,645–21,655.
- Gedalin, M., and M. Balikhin (2004), Electric potential in the low-Mach-number quasi-perpendicular collisionless shock ramp revisited, *J. Geophys. Res.*, *109*, A03106, doi:10.1029/2003JA010219.
- Gedalin, M., and M. Balikhin (2008), Rankine-Hugoniot relations for shocks with demagnetized ions, *J. Plasma Phys.*, *74*, 207–214.
- Greenstadt, E. W., C. T. Russell, F. L. Scarf, V. Formisano, and M. Neugebauer (1975), Structure of the quasi-perpendicular laminar bow shock, *J. Geophys. Res.*, *80*, 502–514.
- Hellinger, P. (2003), Structure and stationarity of quasi-perpendicular shocks: Numerical simulations, *Planet. Space Sci.*, *51*, 649–657.
- Horbury, T. S., P. J. Cargill, E. A. Lucek, A. Balogh, M. W. Dunlop, T. M. Oddy, C. Carr, P. Brown, A. Szabo, and K.-H. Fornacon (2001), Cluster magnetic field observations of the bowshock: Orientation, motion and structure, *Ann. Geophys.*, *19*, 1399–1409.
- Horbury, T. S., P. J. Cargill, E. A. Lucek, J. Eastwood, A. Balogh, M. W. Dunlop, K.-H. Fornacon, and E. Georgescu (2002), Four spacecraft measurements of the quasiperpendicular terrestrial bow shock: Orientation and motion, *J. Geophys. Res.*, *107*(A8), 1208, doi:10.1029/2001JA000273.
- Krasnoselskikh, V., et al. (2013), The dynamic quasiperpendicular shock: Cluster discoveries, *Space Sci. Rev.*, doi:10.1007/s11214-013-9972-y, in press.
- Krauss-Varban, D., Y. Li, and J. G. Luhmann (2008), Ion acceleration at the Earth's bow shock and at interplanetary shocks: A comparison, in *Particle Acceleration and Transport in the Heliosphere and Beyond: 7th Annual International Astrophysics Conference, AIP Conf. Proc.*, *1039*, edited by G. Li et al., pp. 307–313.
- Lefebvre, B., Y. Seki, S. J. Schwartz, C. Mazelle, and E. A. Lucek (2009), Reformation of an oblique shock observed by Cluster, *J. Geophys. Res.*, *114*, A11107, doi:10.1029/2009JA014268.
- Lembège, B., and P. Savoini (1992), Nonstationarity of a two-dimensional quasiperpendicular supercritical collisionless shock by self-reformation, *Phys. Fluids B*, *4*, 3533–3548.
- Lembège, B., P. Savoini, P. Hellinger, and P. M. Trávníček (2009), Nonstationarity of a two-dimensional perpendicular shock: Competing mechanisms, *J. Geophys. Res.*, *114*, A03217, doi:10.1029/2008JA013618.
- Li, X., H. R. Lewis, J. LaBelle, T.-D. Phan, and R. A. Treumann (1995), Characteristics of the ion pressure tensor in the Earth's magnetosheath, *Geophys. Res. Lett.*, *22*, 667–670.
- Lobzin, V. V., V. V. Krasnoselskikh, J.-M. Bosqued, J.-L. Pinçon, S. J. Schwartz, and M. Dunlop (2007), Nonstationarity and reformation of high-mach-number quasiperpendicular shocks: Cluster observations, *Geophys. Res. Lett.*, *34*, L05107, doi:10.1029/2006GL029095.
- Lobzin, V. V., V. V. Krasnoselskikh, K. Musatenko, and T. Dudok de Wit (2008), On nonstationarity and rippling of the quasiperpendicular zone of the Earth bow shock: Cluster observations, *Ann. Geophys.*, *26*, 2899–2910.
- Lowe, R. E., and D. Burgess (2003), The properties and causes of rippling in quasi-perpendicular collisionless shock fronts, *Ann. Geophys.*, *21*, 671–679.
- Matsukiyo, S., and M. Scholer (2006), On reformation of quasi-perpendicular collisionless shocks, *Adv. Space Res.*, *38*, 57–63.
- Mazelle, C., B. Lembège, A. Morgenthaler, K. Meziane, T. S. Horbury, V. Génot, E. A. Lucek, and I. Dandouras (2010), Self-reformation of the quasi-perpendicular shock: CLUSTER observations, in *Proceedings of the Twelfth International Solar Wind Conference, AIP Conf. Proc.*, *1216*, edited by M. Maksimovic et al., pp. 471–474.
- Moullard, O., D. Burgess, T. S. Horbury, and E. A. Lucek (2006), Ripples observed on the surface of the Earth's quasi-perpendicular bow shock, *J. Geophys. Res.*, *111*, A09113, doi:10.1029/2005JA011594.
- Newbury, J. A., C. T. Russell, and M. Gedalin (1998), The ramp widths of high-Mach-number, quasi-perpendicular collisionless shocks, *J. Geophys. Res.*, *103*, 29,581–29,594.
- Ofman, L., M. Balikhin, C. T. Russell, and M. Gedalin (2009), Collisionless relaxation of ion distributions downstream of laminar quasi-perpendicular shocks, *J. Geophys. Res.*, *114*, A09106, doi:10.1029/2009JA014365.
- Ofman, L., and M. Gedalin (2013), Two-dimensional hybrid simulations of quasi-perpendicular collisionless shock dynamics: gyrating downstream ion distributions, *J. Geophys. Res. Space Physics*, *118*, 1828–1836, doi:10.1029/2012JA018188.
- Russell, C. T., M. M. Hoppe, W. A. Livesey, J. T. Gosling, and S. J. Bame (1982), ISEE-1 and -2 observations of laminar bow shocks: Velocity and thickness, *Geophys. Res. Lett.*, *9*, 1171–1174.
- Russell, C. T., L. K. Jian, X. Blanco-Cano, and J. G. Luhmann (2009), STEREO observations of upstream and downstream waves at low Mach number shocks, *Geophys. Res. Lett.*, *36*, L03106, doi:10.1029/2008GL036991.
- Savoini, P., and B. Lembege (1994), Electron dynamics in two- and one-dimensional oblique supercritical collisionless magnetosonic shocks, *J. Geophys. Res.*, *99*, 6609–6635.
- Schmidt, J. M., and I. H. Cairns (2012), Type II radio bursts: 2. Application of the new analytic formalism, *J. Geophys. Res.*, *117*, A11104, doi:10.1029/2012JA017932.
- Scopke, N., G. Paschmann, S. J. Bame, J. T. Gosling, and C. T. Russell (1983), Evolution of ion distributions across the nearly perpendicular bow shock: Specularly and non-specularly reflected-gyrating ions, *J. Geophys. Res.*, *88*, 6121–6136.
- Scopke, N., G. Paschmann, A. L. Brinca, C. W. Carlson, and H. Lühr (1990), Ion thermalization in quasi-perpendicular shocks involving reflected ions, *J. Geophys. Res.*, *95*, 6337–6352.
- Scudder, J. D., T. L. Aggson, A. Mangeney, C. Lacombe, and C. C. Harvey (1986), The resolved layer of a collisionless, high beta, supercritical, quasi-perpendicular shock wave. I. Rankine-Hugoniot geometry, currents, and stationarity, *J. Geophys. Res.*, *91*, 11,019–11,052.
- Viñas, A. F., and J. D. Scudder (1986), Fast and optimal solution to the “Rankine-Hugoniot problem”, *J. Geophys. Res.*, *91*, 39–58.
- Walker, S. N., M. A. Balikhin, T. L. Zhang, M. E. Gedalin, S. A. Pope, A. P. Dimmock, and A. O. Fedorov (2011), Unusual nonlinear waves in the Venusian magnetosheath, *J. Geophys. Res.*, *116*, A01215, doi:10.1029/2010JA015916.
- Wambecq, A. (1978), Rational Runge-Kutta methods for solving systems of ordinary differential equations, *Computing*, *20*, 333–342.
- Winske, D., and K. B. Quest (1988), Magnetic field and density fluctuations at perpendicular supercritical collisionless shocks, *J. Geophys. Res.*, *93*, 9681–9693.
- Yang, Z. W., B. Lembège, and Q. M. Lu (2012), Impact of the rippling of a perpendicular shock front on ion dynamics, *J. Geophys. Res.*, *117*, A07222, doi:10.1029/2011JA017211.
- Yuan, X., I. H. Cairns, L. Trichtchenko, R. Rankin, and D. W. Danskin (2009), Confirmation of quasi-perpendicular shock reformation in two-dimensional hybrid simulations, *Geophys. Res. Lett.*, *36*, L05103, doi:10.1029/2008GL036675.